Journal of Sol-Gel Science and Technology (2020) 93:535–545
https://doi.org/10.1007/s10971-020-05218-x

ORIGINAL PAPER: NANO-STRUCTURED MATERIALS (PARTICLES, FIBERS, COLLOIDS, COMPOSITES, ETC.)

Adsorption characteristics and electrochemical performance of reactive red onto magnetic $MgFe_2O_4$ nanoparticles prepared via a facile alcohol combustion process

Yunhua Yang[1] · Yafei Zhang[1] · Zhou Wang[2]

Received: 29 August 2019 / Accepted: 6 January 2020 / Published online: 22 January 2020

Abstract

Magnetic $MgFe_2O_4$ nanoparticles were prepared successfully via a facile alcohol combustion process and applied to remove the reactive red (RR) from aqueous solution. Characterizations of the as-prepared $MgFe_2O_4$ nanoparticles were performed by the scanning electron microscopy (SEM), the transmission electron microscope (TEM), the X-ray diffraction (XRD), the vibrating sample magnetometer (VSM), and the Brunauer–Emmett–Teller (BET) measurement. The adsorption characteristics of RR onto $MgFe_2O_4$ nanoparticles at room temperature were investigated. Compared with the pseudo-first-order and intraparticle diffusion model, the pseudo-second-order kinetic model could be applied to evaluate the adsorption performance of RR onto $MgFe_2O_4$ nanoparticles in a range of initial concentration of 100–400 mg/L. Based on the values of the correlation coefficients, the equilibrium experimental data related to the adsorption of RR showed that the adsorption performance followed the Langmuir isotherm model with maximum adsorption capacity of 119.07 mg/g. The obtained results implied that the adsorption mechanism of RR onto $MgFe_2O_4$ nanoparticles at room temperature was the monolayer adsorption.

Graphical Abstract

Magnetic $MgFe_2O_4$ nanoparticles were prepared via the facile alcohol combustion process, and the magnetic $MgFe_2O_4$ nanoparticles were applied to remove the reactive red (RR) from aqueous solution, the adsorption kinetics and adsorption isothermals of RR onto $MgFe_2O_4$ nanoparticles at room temperature were investigated.

✉ Zhou Wang
pzhwangzhou@163.com

[1] Danyang Maternal and Child Health Hospital, Zhenjiang 212300, PR China

[2] College of Vanadium and Titanium, Panzhihua University, Panzhihua 617000, PR China

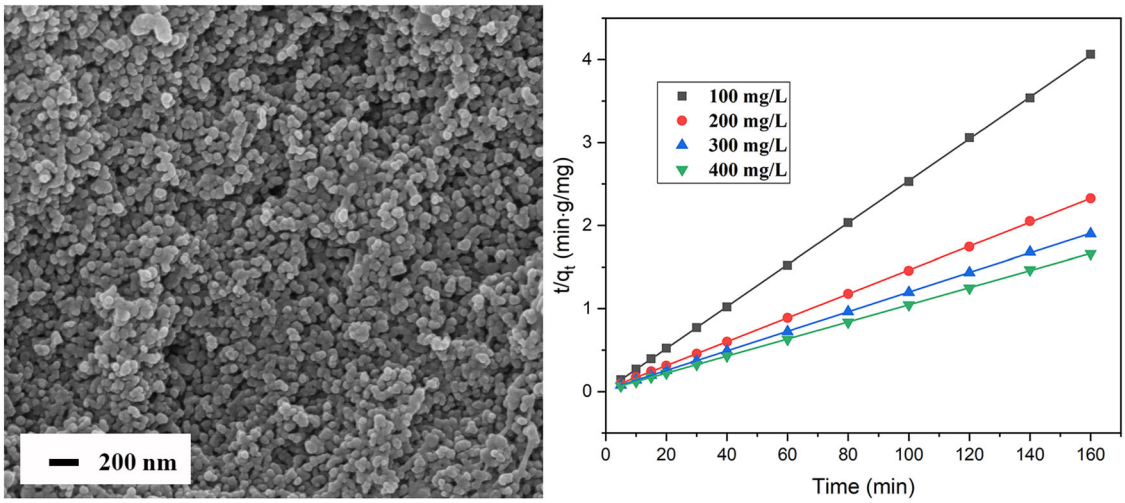

Highlights

- $MgFe_2O_4$ nanoparticles were prepared via the facile alcohol combustion process.
- The pseudo-second-order kinetics model can explain the adsorption process of RR onto them.
- The adsorption isotherm of RR onto them at room temperature conformed to Langmuir model.

Keywords $MgFe_2O_4$ nanoparticles Alcohol combustion · Reactive red Adsorption kinetics · Adsorption isotherm

1 Introduction

Dye is one of the major sources of environment pollutions. In cosmetics, food, leather, paper, and textile industries various dyes are frequently applied as colorants to process products and factories often discharge large amounts of contaminants containing dyes into the aquatic ecosystem. The presence of these dyes in ambient environment threats the environmental sustainability due to massive discharge of wastewater. Dyes' wastewater will cause allergic, carcinogenic, mutagenic and toxic hazards to biological organisms, which is even harmful to the survival and development of plants, animals, and humans [1, 2]. Hence, it is urgent to remove dye from industries' effluents. The dye uptakes in wastewaters have always been a troublesome problem for the environment protection. The treatment for dyes' wastewaters is difficult due to complex and varied water bodies that contain large quantity of organic and inorganic dyes [3]. Various techniques for removing dyes from the wastewater have been developed, the most common techniques of dye treatment include coagulation, oxidation, adsorption, reverse osmosis, and so forth. In addition to the employ of organic solvents and cumbersome operation, these techniques can also cause damage to equipment, resulting in costly repair costs. Nevertheless, the adsorption as a treatment technology of industrial wastewater has displayed effective and promising result, because of its advantages of high efficiency, simple control process, cost-effectiveness, and environmental-friendliness [4, 5].

Various adsorbents, such as peanut shell [6], chitosan [7], and mesoporous activated carbon [8], have been intensively investigated for the removal of dyes. They involve defects of the high treatment costs, sluggish kinetics, low adsorption capacity, and so on, thus limiting further applications. In order to enhance the removal efficiency, various nanoadsorbents are studied and applied to adsorb dye with the development of nanomaterials, and they represent a high adsorption capacity [9, 10]. Compared with nonmagnetic adsorbents, magnetic nanomaterials that are easy to separate from aqueous solutions, have been gaining attention as a recyclable absorbent. Most of the previous studies indicate that the magnetic adsorbents have many advantages such as excellent mechanical properties, large specific surface area, facile separation, and high recycling performance. The numerous active sites of magnetic nanomaterials make the theoretically extraordinary application potential in adsorption. It is worthy that the magnetic nanoabsorbents are considered as a highly efficient adsorbent for organic and inorganic substances [11].

As adsorbent to remove dyes, magnetic $MgFe_2O_4$ nanoparticle is one of the significant nanomaterials due to its excellent adsorption performance. Many approaches have been developed to fabricate $MgFe_2O_4$ nanoparticles, such as the autoclave route [12], the hydrothermal process [13, 14], the sol–gel method [15], the glycine–nitrate method [16], etc. The preparation procedures of the above approaches have been limited by the long pretreatment processes, use of toxic solvents, expensive devices. However, the alcohol

combustion technique is introduced as a convenient, facile, and novel method, which provides the advantages of low cost, short preparation period, homogeneous products, and free of dispersants [17–20].

In this project, we have successfully prepared the magnetic $MgFe_2O_4$ nanoparticles via the facile alcohol combustion process, and the adsorption characteristics and the electrochemical performance of reactive red (RR) onto them was investigated.

2 Experimental details

2.1 Preparation and characteristics of magnetic $MgFe_2O_4$ nanoparticles

The magnetic $MgFe_2O_4$ nanoparticles were prepared via the alcohol-assisted combustion process. Typically, analytical grade magnesium nitrate and iron nitrate were used, and the molar ratio of Mg and Fe was 1:2. a mixture of 2.56 g of Mg $(NO_3)_2{\cdot}6H_2O$ and 8.08 g of $Fe(NO_3)_3{\cdot}9H_2O$ were dispersed in 20 mL of absolute ethyl alcohol, the mixture was maintained at room temperature with constant stirring for 1 h to form the homogeneous solution, which subsequently was put into a crucible and ignited. Ignition combustion process replaced the process of forming xerogel in traditional sol–gel method, which significantly reduced the preparation time [21]. After the flame was extinguished, the gel was obtained in the crucible. Crucible with obtained gel was placed in the calciner with the heat rate of 3 °C/min; it was kept at 600 °C for 2 h to form $MgFe_2O_4$ nanoparticles that were applied as adsorbent for RR removal. X-ray diffraction (XRD) pattern of the as-synthesized nanoparticles was collected with Holland Philips X'Pert X-ray diffractometer (Cu Ka radiation, $\lambda = 1.5406$ Å, 30 mA and 40 kV) for 2θ over 20°–80°. The morphology and structure studies were performed by SEM and TEM techniques. Magnetic saturation experiment was carried out using a vibrating sample magnetometry (VSM) with a maximum magnetic field of 10 kOe. The Brunauer–Emmett–Teller (BET) surface area via nitrogen adsorption was determined with the instrument of NOVA 2000e.

2.2 Adsorption performance of RR onto $MgFe_2O_4$ nanoparticles

Adsorption experiments were performed in a batch of 50 mL flasks and the flasks were shaken for the required contact time. In kinetics experiment, an average of 0.05 g of magnetic $MgFe_2O_4$ nanoparticles was added to RR aqueous solution (20 mL) with the initial concentration of 100–400 mg/L. The suspensions were agitated. Then, the flasks were taken out at predetermined time intervals, the adsorbents were separated under the magnetic field and the residual RR amounts in the solution was determined by measuring the absorbance. To study the adsorption isotherms, the experiments were carried out by mixing 0.05 g of magnetic $MgFe_2O_4$ nanoparticles and 20 mL RR with various concentrations in flasks, these flasks were maintained at room temperature and agitated. The supernatant was collected after reaching equilibrium. The absorbance of RR at 530 nm was investigated by UV spectrophotometer (UV-2250).

The adsorption capacity of the $MgFe_2O_4$ nanoparticles for RR could be calculated by the following [22]:

$$q = \frac{(C_0 - C_t) \cdot V}{m}, \tag{1}$$

where C_0 (mg/L) and C_t (mg/L) referred the initial concentration of RR solution and the concentration for any time, respectively; m represented the weight of $MgFe_2O_4$ nanoparticles (g), V was the volume of RR solution.

2.3 Electrochemical measurement

The electrodes were constructed using a three-electrode system. The platinum wire and $Ag/AgCl_2$ were used as counter and reference electrode, respectively. During preparation process of working electrodes, magnetic $MgFe_2O_4$ nanoparticles and post adsorption nanoparticles were mixed in aqueous solution at concentration of 1 mg/mL. The 2 μL solution was coated in the center of the magnetic glassy carbon electrode (MGCE), and the samples were placed in a vacuum oven to dry at 30 °C. The bare MGCE, as-prepared magnetic $MgFe_2O_4$ nanoparticles and post adsorption nanoparticles were applied as work electrode to measure the electrochemical property. The experiments of cyclic voltammetry (CV, potential range from −0.2 to 0.6 V, scan rate of 0.1 V/s) and electrochemical impedance spectroscopy (EIS, frequency range of 1–10^4 Hz, amplitude of 5 mV) were performed using an electrochemical workstation (CHI660E).

3 Results and discussion

3.1 Characterization of $MgFe_2O_4$ nanoparticles

The characteristics of magnetic $MgFe_2O_4$ nanoparticles calcined at 600 °C for 2 h with absolute alcohol of 20 mL were evinced in Fig. 1. Figure 1a showed the SEM micrograph of magnetic $MgFe_2O_4$ nanoparticles' microstructure, and it was clear that the average diameter of nanoparticles was around 120 nm and the size distribution was comparatively uniform, however there was a certain degree of aggregation between the particles. Figure 1b illustrated the TEM image of $MgFe_2O_4$ nanoparticles, obviously, the $MgFe_2O_4$ nanoparticles had a polycrystalline structure, and the grain size was around

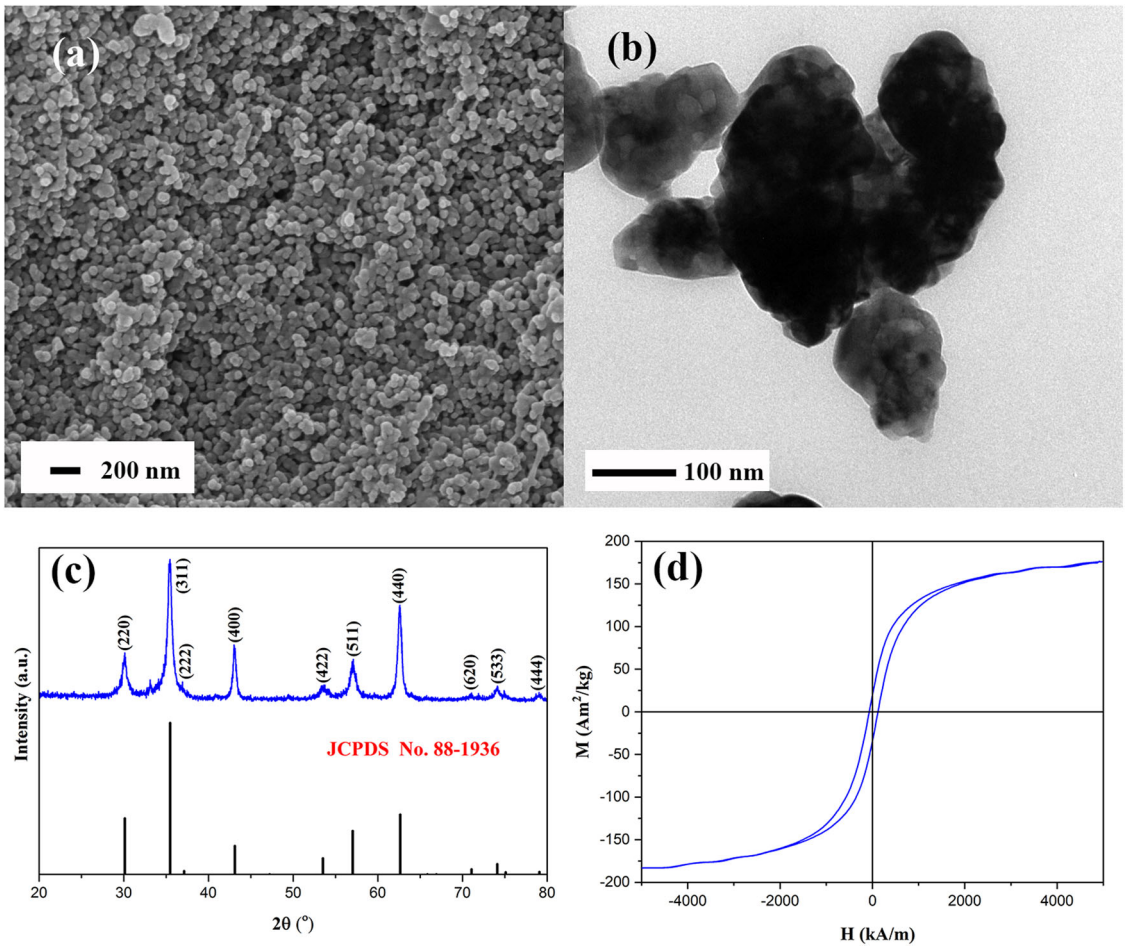

Fig. 1 SEM (**a**), TEM (**b**), XRD (**c**), and VSM (**d**) of magnetic $MgFe_2O_4$ nanoparticles calcined at 600 °C for 2 h with absolute alcohol of 20 mL

120 nm, which was in accordance with the SEM morphology. The XRD pattern of $MgFe_2O_4$ nanoparticles was displayed in Fig. 1c, when the calcination temperature was at 600 °C for 2 h, the diffraction peaks of $MgFe_2O_4$ nanoparticles matched well with (220), (311), (222), (400), (422), (511), (440), (620), (533), and (444) planes, the result indicated that crystal structure-obtained products were single-phase spinel $MgFe_2O_4$ (JCPDS No. 88-1936). The average crystallite size (D) of $MgFe_2O_4$ nanoparticles could be calculated from the value of full-width (FWHM) at half-maximum of (311) plane by Scherrer's formula [18]. The average crystallite size of $MgFe_2O_4$ was determined to be 32 nm, which was smaller than particle sizes observed in TEM and SEM images. The reason was that $MgFe_2O_4$ nanoparticles were formed by the aggregation of multiple crystals. The hysteresis loop of the $MgFe_2O_4$ nanoparticles was exhibited in Fig. 1d, it could be observed that the saturation magnetization (*Ms*) of magnetic $MgFe_2O_4$ nanoparticles was 176.2 Am^2/kg with a typical soft magnetization behavior.

The BET measurement for the magnetic $MgFe_2O_4$ nanoparticles was shown in Fig. 2. It could be seen that the curve belonged to the IV nitrogen adsorption isotherm whose adsorption curve was not coincidence with desorption curve, thus forming a hysteresis loop. This nitrogen adsorption–desorption isotherm exhibited the adsorption and desorption behavior of porous materials. The specific surface area was calculated as 33.4 m^2/g, and the estimated pore size distribution was shown in the inset of Fig. 2, it could be observed that the pore size was concentrated at 4 nm, which led a larger specific surface area. Both large surface area and highly porous structure provided more adsorption sites for the material, which were beneficial for dye removal.

3.2 Adsorption of RR onto magnetic $MgFe_2O_4$ nanoparticles

3.2.1 Adsorption kinetics

In order to better design the treatment process from sewage, it is significant to evaluate the removal efficiency of pollutants in aqueous solution. The experimental data obtained from RR kinetic experiments were fitted using pseudo-first-

order model [7], pseudo-second-order model [23], and the intraparticle diffusion model [24, 25], and the adsorption mechanism of RR adsorption onto magnetic $MgFe_2O_4$ nanoparticles was explicated. The three equations of kinetic model were represented as follows:

$$q_t = q_e\left(1 - e^{-k_1 t}\right), \tag{2}$$

$$q_t = \frac{q_e^2 k_2 t}{1 + q_e k_2 t}, \tag{3}$$

$$q_t = c_i + k_i t^{1/2}, \tag{4}$$

where k_1, k_2, and k_i represented the rate constants of the pseudo-first-order model, the pseudo-second-order kinetic model, and the intraparticle diffusion models, q_e (mg/g) was the adsorbed RR amounts at equilibrium state, q_t (mg/g) was associated to adsorption capacity at any time, c_i was boundary layer thickness.

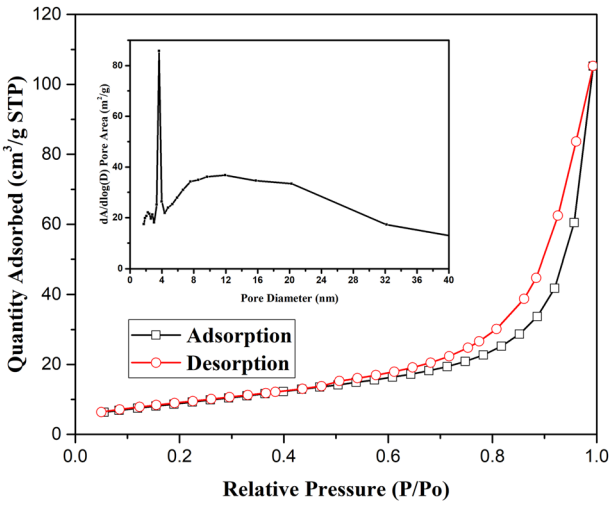

Fig. 2 Nitrogen sorption isotherm of magnetic $MgFe_2O_4$ nanoparticles calcined at 600 °C for 2 h with absolute alcohol of 20 mL

Origin software was applied to fit all the models, and the accurate theoretical model was selected to describe the adsorption behavior of RR onto magnetic $MgFe_2O_4$ nanoparticles based on the correlation coefficient (R^2) values as indicator, which better represented the experimental data. The experimental data of RR solution at different concentrations were respectively fitted by the pseudo-first-order, the pseudo-second-order, and the intraparticle diffusion models. The kinetic parameters of the relevant fitting models were summarized in Table 1. The fitting effects of the models were evaluated by correlation coefficients (R^2). It could be observed that R^2 value of pseudo-second-order kinetic exceeded 0.98 at diverse RR concentrations (100, 200, 300, 400 mg/L). As shown in Fig. 3, The high value of R^2 suggested that the kinetics of RR onto magnetic $MgFe_2O_4$ nanoparticles followed the pseudo-second-order kinetic model and hence not a diffusion-controlled phenomenon.

Figure 4 showed the experimental data at predetermined contact time and fitted curve of pseudo-second-order kinetics model under different concentrations of RR. As displayed in Fig. 4, the adsorption process would be affected by initial RR concentration. The adsorption capacity of RR onto magnetic $MgFe_2O_4$ nanoparticles drastically increased during the initial stage of adsorption and then increased at a slow rate until equilibrium was reached after 60 min, which might be due to more vacancies on the surface of the adsorbent at the initial stage. When the initial concentration of RR was 400 mg/L, the adsorption capacity could reach 96.9 mg/g. Figure 5 showed the linear fits of the pseudo-second-order kinetics model, and the relative errors for the experimental q_e and q_e calculated from the Eq. (3) were <0.4%, which implied that the experimental data followed the regularity of pseudo-second-order kinetic model and there was excellent linear relation between them. The pseudo-second-order adsorption kinetics model included all processes of adsorption namely, extra-granular diffusion, outer surface adsorption, intraparticle diffusion, and internal surface adsorption. $MgFe_2O_4$ nanoparticles had small

Table 1 Fitted kinetics parameters for adsorption of RR from aqueous solutions onto magnetic $MgFe_2O_4$ nanoparticles

Kinetic models	Equations	Parameters	RR concentration (mg/L)			
			100	200	300	400
Pseudo-first-order model	$q_t = q_e\left(1 - e^{-k_1 t}\right)$	q_e (mg/g)	38.9716	66.9093	81.6458	93.4410
		k_1	0.4474	0.2419	0.2750	0.2852
		Adj. R^2	0.7164	0.7921	0.7426	0.7116
Pseudo-second-order model	$q_t = \frac{q_e^2 k_2 t}{1+q_e k_2 t}$	q_e (mg/g)	39.6735	69.7084	84.7436	96.9505
		k_2	0.0383	0.0073	0.0071	0.0065
		Adj. R^2	0.9875	0.9848	0.9865	0.9845
Intraparticle diffusion model	$q_t = C_i + k_i t^{\frac{1}{2}}$	C_i	36.4384	55.0251	69.0548	79.3371
		k_i	0.2938	1.3115	1.4152	1.6004
		Adj. R^2	0.5895	0.6437	0.6630	0.6922

particle sizes, large specific surface areas, and a certain surface energy, and the adsorption between the adsorbent, and the adsorbate was caused by an intermolecular force.

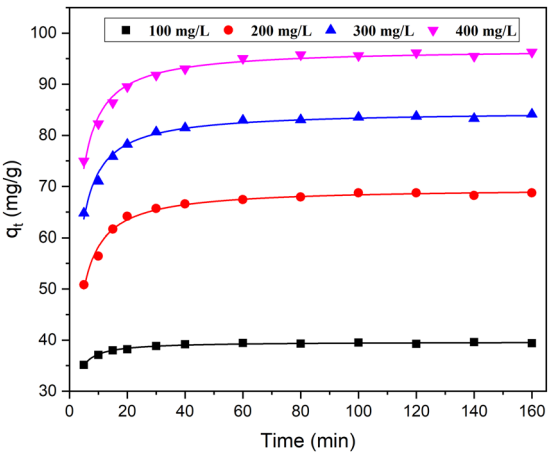

Fig. 3 Pseudo-second-order kinetic model for adsorption of RR onto magnetic $MgFe_2O_4$ nanoparticles at various initial concentrations

The adsorption process of dye first occurred on the surface of $MgFe_2O_4$ nanoparticles by van der Waals force and hydrogen bonding, then partial dye molecules by anionic groups were electrostatically attracted with positively charged $MgFe_2O_4$ nanoparticles. In addition, ion exchange or other chemical forces may be present during the adsorption process. Therefore, the adsorption process had both physical adsorption and chemical adsorption.

3.2.2 Adsorption isotherms

Adsorption isotherm was vital to describe how adsorbent surface interacted with molecules of adsorbate. Therefore, the experimental data of RR adsorption equilibrium on $MgFe_2O_4$ nanoparticles was interpreted using theoretical equation. The models of Langmuir, Freundlich, and Temkin were applied for the analysis of equilibrium data.

The theoretical model of Langmuir isotherm assumed that the adsorbent surface was homogeneously covered by a monolayer of the adsorbate. The adsorption energy was

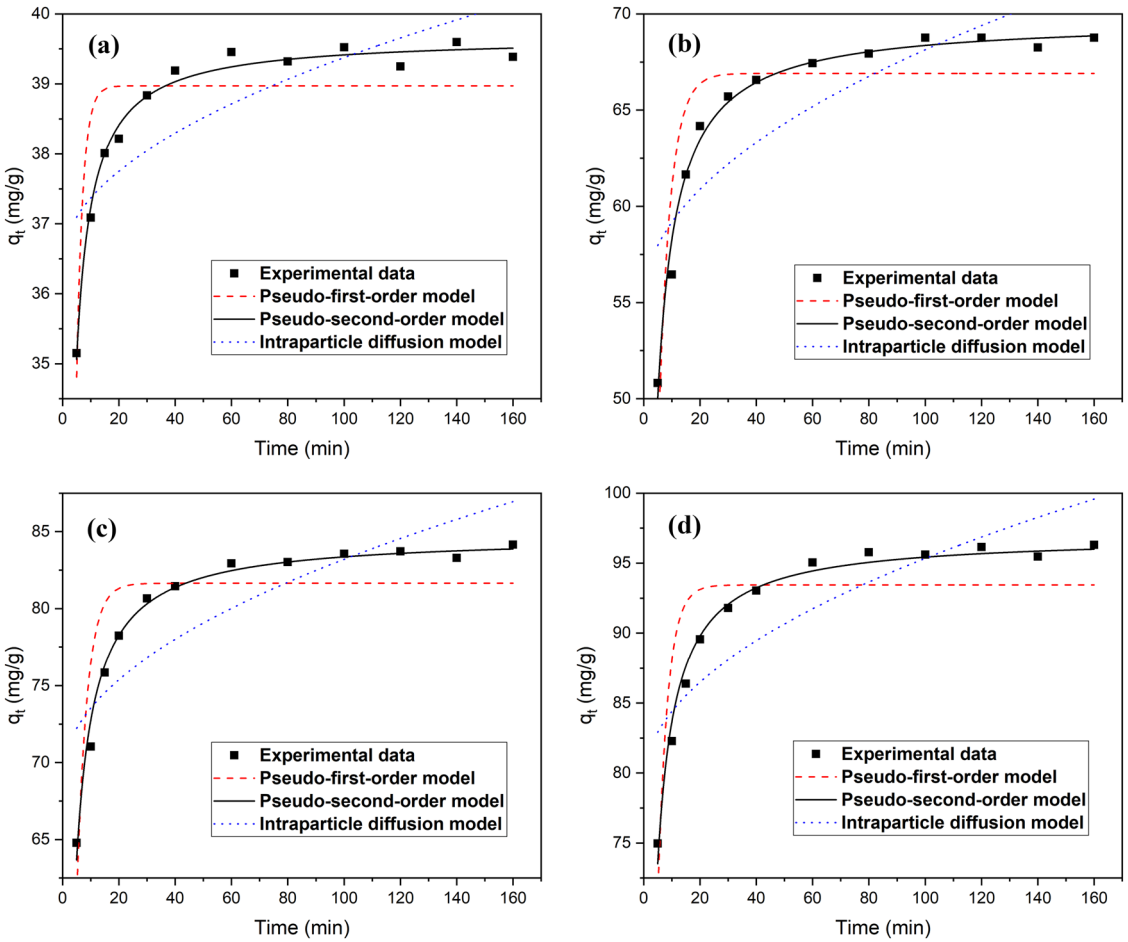

Fig. 4 Fits of the pseudo-first-order kinetics model, pseudo-second-order kinetics model and intraparticle diffusion kinetics model at initial RR concentrations of 100 mg/L (**a**), 200 mg/L (**b**), 300 mg/L (**c**), 400 mg/L (**d**)

uniformly dispersed on the adsorbent surface consisted of active sites and was constant, surface heterogeneity of the adsorbent was not taken into account in this model. The equation of Langmuir model was represented as [26]

$$q_e = \frac{q_{\max} K_L C_e}{1 + K_L C_e}, \tag{5}$$

where q_e (mg/g) was the equilibrium adsorption capacity of RR onto magnetic $MgFe_2O_4$ nanoparticles, $q_{\max}$ (mg/g) gave an idea of the maximum adsorption capacity in theory, K_L (L/mg) represented Langmuir constant related to the adsorption rate of the adsorbent.

The Freundlich adsorption isotherm presumed that the adsorption process of multilayer took place on heterogeneous surface of adsorbent. The multilayer adsorption of active sites with heterogeneous energetic distribution and interaction between adsorbed molecules should be further considered. This empirical equation was mostly applied to describe the adsorption of inorganic and organic components in solution, expressed by the following equation [27]:

$$q_e = K_F C_e^{1/n}, \tag{6}$$

where K_F ($mg{\cdot}L^{1/n}{\cdot}mg^{-1/n}{\cdot}g^{-1}$) was isotherm constant that reflected the adsorption capacity. The 1/n value ranging from 0 to 1 represented dimensionless factor related to adsorption intensity.

The Temkin isotherm model took into account the effects of the interaction between adsorbent and adsorbate. As the coverage area of the adsorbate increased, the heat of the adsorbent encapsulated inside decreased constantly. and the binding energy was uniformly distributed during the adsorption process, reaching a certain maximum. The Temkin adsorption isotherm expression was expressed as follows [28]:

$$q_e = B \ln(A_T C_e), \tag{7}$$

where B (=RT/b_T) was the Temkin constant related to adsorption heat, A_T (L/g) was equilibrium binding constant corresponding to maximum binding energy, T (K) represented the absolute solution temperature, and R ($8.314 J{\cdot}mol^{-1}{\cdot}K^{-1}$) was the universal gas constant.

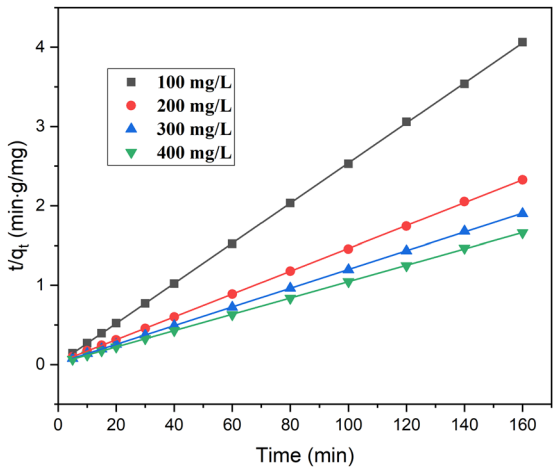

Fig. 5 Linear fits of the pseudo-second-order kinetics model at initial RR concentrations of 100–400 mg/L

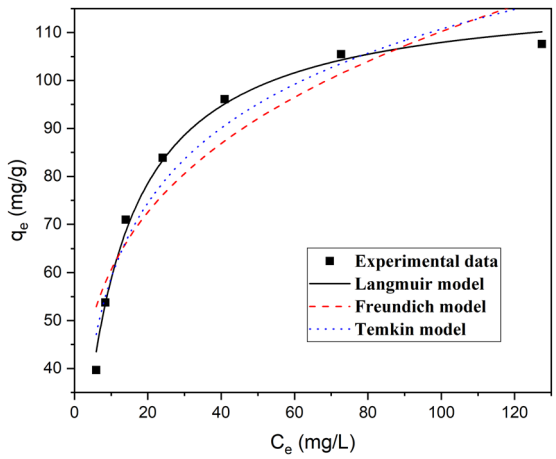

Fig. 6 The Langmuir, Freundlich, and Temkin isotherms for adsorption of RR onto magnetic $MgFe_2O_4$ nanoparticles at room temperature

Figure 6 exhibited the experimental plot and fitted curves of Langmuir, Freundlich, and Temkin models. The relevant parameters (K_L, $q_{\max}$, K_F, $1/n$, A_T, and B) obtained from the three isotherm models were calculated and summarized in Table 2. By comparing the values of the correlation coefficients (R^2) between the isotherm models, the Langmuir isotherm model could give the highest R^2 value that exceeded 0.99. The Langmuir yielded the best fit ($R^2 = 0.9912$). While, the R^2 values of Freundlich and Temkin isotherm ($R^2 = 0.8634$, 0.9374) were relatively lower, which indicated that the adsorption of RR onto magnetic $MgFe_2O_4$ nanoparticles could be best described by Langmuir model. The mechanism of Langmuir isotherm suggested that the adsorption process of the RR occurred at a specific site on the surface of the $MgFe_2O_4$ nanoparticles. When the homogeneous sites were occupied, the adsorption couldn't produce in the same site.

3.3 Effect of pH on adsorption

The pH in solution was a crucial factor affecting the removal efficiency of adsorbents. Adsorption experiments were performed in the range of solutions pH from 5 to 9. Figure 7 showed the effects of pH on adsorption for $MgFe_2O_4$ nanoparticles calcined at 600 °C for 2 h with absolute alcohol of 20 mL, it could be seen that the adsorption capacity firstly improved until 7 of pH value and then dropped sharply with further increase of pH value. The phenomenon was caused by

Table 2 Evaluated model parameters of adsorption isotherms for RR onto magnetic $MgFe_2O_4$ nanoparticles at room temperature

Model	Equation	Adj. R^2	Parameters	Parameters value
Langmuir	$q_e = \frac{q_{max} K_L C_e}{1+K_L C_e}$	0.9912	q_{max}	119.0717
			K_L	0.0969
Freundlich	$q_e = K_F C_e^{\frac{1}{n}}$	0.8634	K_F	33.2826
			$\frac{1}{n}$	0.2600
Temkin	$q_e = B \ln(A_T C_e)$	0.9374	B	22.5246
			A_T	1.3638

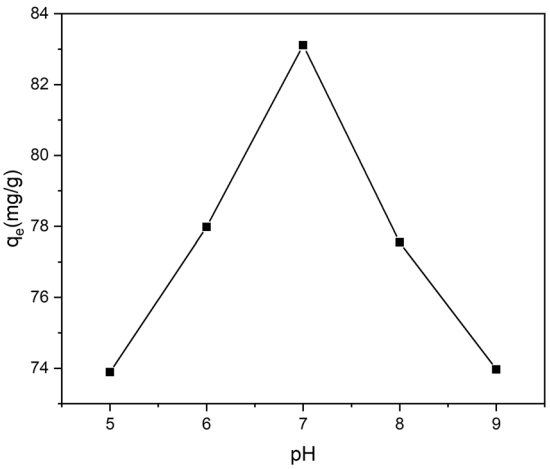

Fig. 7 Effect of pH on the adsorption of RR onto magnetic $MgFe_2O_4$ nanoparticles

Table 3 Comparison of the adsorption capacity of RR dye on various adsorbents

Adsorbents	q_{max} (mg·g^{-1})	Reference
Cross-linked chitosan–GLA/TiO_2 nanocomposite	103.1	[30]
Functionalized sludge	46.8	[31]
Jatropha curcas shell treated by non-thermal plasma	85.3	[32]
Cross-linked chitosan–ethylene glycol diglycidyl ether	165.3	[33]
Cetylpyridinium modified resadiye bentonite	81.9	[34]
Fe_3O_4 nanoparticles	166.6	[35]
Chitosan coacervated particles	82.1	[36]
Chitosan/zeolite composite	35.57	[37]
$MgFe_2O_4$ nanoparticles	119.1	This work

electrostatic interaction of $MgFe_2O_4$ nanoparticles and ionized dye. When the pH of solution was less than RR isoelectric point that was about 7, the positive charge of RR increased as the pH decreased. The electrostatic repulsion was enhanced between RR and positively charged $MgFe_2O_4$, which would cause a reduction in the removal efficiency of RR. When pH was greater than 7 in solution, hydroxide ions were generated and dye had negative charge. Meanwhile, the activated surface sites of $MgFe_2O_4$ nanoparticles would produce electrostatic attraction to hydroxide ions. The emergence of competitive adsorption limited the removal of RR between hydrogen ions and the dye. The above results indicated that the pH of solution was a vital driving force for whole adsorption phase, and the variation of pH disturbed the situation to which the ionized dye molecules transported electrostatic charges.

The performance comparison in terms of adsorption capacities of the RR dye on various adsorbents was presented in Table 3. It could be seen that the adsorbent reported in this study had a relatively high adsorption capacity in comparison with all of the other adsorbents. Magnetic $MgFe_2O_4$ nanoparticles not only had higher adsorption ability for RR dye, but also had facile magnetic separation ability. Magnetization and availability of more active adsorption sites indicated that $MgFe_2O_4$ nanoparticles could be considered a convenient and effective adsorbent in wastewater treatment.

3.4 Magnetic response test

Figure 8 showed photograph of magnetic $MgFe_2O_4$ nanoparticles adsorption behavior and magnetic separation process. Figure 8a displayed RR solution with the concentration of 200 mg/L, while Fig. 8b showed that magnetic $MgFe_2O_4$ nanoparticles had good dispersion in RR solution, and Fig. 8c provided the magnetic separation image of $MgFe_2O_4$ nanoparticles from RR solution, which indicated strong adsorption effect of $MgFe_2O_4$ nanoparticles to RR, and the nanoparticles adsorbed dye could be effectively separated under the external magnetic field.

3.5 Electrochemical properties

In order to evaluate electrochemical properties of magnetic $MgFe_2O_4$ nanoparticles before and after RR adsorption. Electrochemical performance changes of bare MGCE, MGCE/$MgFe_2O_4$ and MGCE/post adsorption nanoparticles were further investigated. The CV analysis of the three samples were displayed in Fig. 9a, it could be

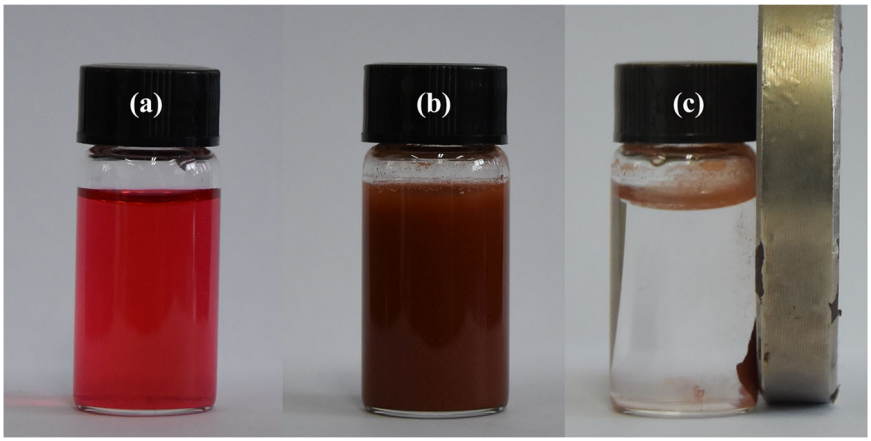

Fig. 8 Photograph of magnetic $MgFe_2O_4$ nanoparticles adsorption behavior and magnetic separation process: 200 mg/L RR solution (**a**), RR solution with $MgFe_2O_4$ nanoparticles (**b**), magnetic separation of magnetic $MgFe_2O_4$ nanoparticles after adsorption of RR for 12 h (**c**)

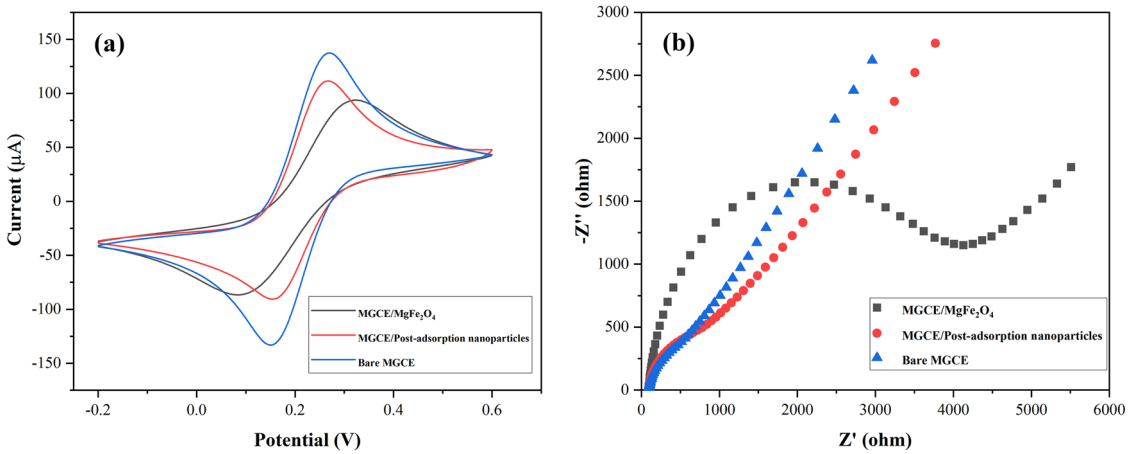

Fig. 9 CV analysis (**a**) and EIS (**b**) of bare MGCE, MGCE/$MgFe_2O_4$ and MGCE/post adsorption nanoparticles

observed that the peak currents of the bare MGCE were larger than the MGCE/post adsorption nanoparticles. While for the response on the MGCE/$MgFe_2O_4$ nanoparticles, the corresponding peak was widest and the peak currents were minimal. The curve of EIS consisted of arc and straight line, the radius of the arc represented the resistance degree to the electron transfer from the electrode. The linear part at region of low frequency was related to the limited rate step of diffusion [29]. As exhibited in Fig. 9b, the maximum radius of MGCE/$MgFe_2O_4$ nanoparticles could be seen, that clearly indicated that MGCE/$MgFe_2O_4$ nanoparticles had maximum resistance. Which was consistent with the CV consequence in Fig. 9a. These results confirmed that the RR successfully occupied the surface sites of the magnetic $MgFe_2O_4$ nanoparticles.

4 Conclusions

(1) Magnetic $MgFe_2O_4$ nanoparticles were prepared successfully via the facile alcohol combustion process, and the magnetic $MgFe_2O_4$ nanoparticles calcined at 600 °C for 2 h with 20 mL of absolute alcohol were characterized with average particle size of around 120 nm and the specific magnetization of 176.2 Am^2/kg.

(2) The kinetic parameters of pseudo-first-order, the pseudo-second-order, and the intraparticle diffusion models for various initial concentrations from 100 to 400 mg/L were calculated. The adsorption process of RR from aqueous solutions onto the magnetic $MgFe_2O_4$ nanoparticles followed pseudo-second-order model.

(3) Analysis of equilibrium data indicated that the Langmuir model could describe the adsorption mechanism of RR onto the magnetic $MgFe_2O_4$ nanoparticles, which was dominated by monolayer adsorption.

Acknowledgements This work was supported by the Opening Project of Key Laboratory of Green Chemistry of Sichuan Institutes of Higher Education (LYJ1910).

Compliance with ethical standards

Conflict of interest The authors declare that they have no conflict of interest.

References

1. Nguyen CH, Juang RS (2019) Efficient removal of methylene blue dye by a hybrid dsorption-photocatalysis process using reduced graphene oxide/titanate nanotube composites for water reuse. J Ind Eng Chem 76:296–309
2. Pan S, Huang W, Yu QM, Liu X, Liu YH, Liu RJ (2019) A rapid combustion process for the preparation of $Ni_xCu_{1-x}Fe_2O_4$ nanoparticles and their adsorption characteristics of methyl blue. Appl Phys A Mater. https://doi.org/10.1007/s00339-019-2390-6
3. Yu Y, Qiao N, Wang DJ, Zhu QZ, Fu F, Cao RQ, Wang R, Liu W, Xu B (2019) Fluffy honeycomb-like activated carbon from popcorn with high surface area and well-developed porosity for ultra-high efficiency adsorption of organic dyes. Bioresource Technol. https://doi.org/10.1016/j.biortech.2019.121340
4. Chen JX, Jiang MH, Han J, Liu K, Liu ML, Wu, Q (2019) Syntheses of magnetic GO@melamine formaldehyde resin for dyes adsorption. Mater Res Express. https://doi.org/10.1088/2053-1591/ab1ba6
5. Chen YX, Jing C, Zhang X, Jiang DB, Liu XY, Dong BQ, Feng L, Li SC, Zhang YX (2019) Acid-salt treated CoAl layered double hydroxide nanosheets with enhanced adsorption capacity of methyl orange dye. J Colloid Inter Sci 548:100–109
6. Du X, Yan H, Dai YJ (2017) Adsorption behavior of neutral red from aqueous solution onto NaOH-modified peanut shell. Fresen Environ Bull 26:4522–4527
7. Wang JQ, Zhou QS, Song DQ, Qi B, Zhang YJ, Shao YZ, Shao ZQ (2015) Chitosan-silica composite aerogels: preparation, characterization and Congo red adsorption. J Sol-Gel Sci Techn 76 (3):501–509
8. Lorenc-Grabowska E, Gryglewicz G (2007) Adsorption characteristics of Congo Red on coal-based mesoporous activated carbon. Dyes Pigments 74:34–40
9. Adhikari S, Mandal S, Sarkar D, Kim DH, Madras G (2017) Kinetics and mechanism of dye adsorption on WO_3 nanoparticles. Appl Surf Sci 420:472–482
10. Tian Y, Zhong S, Zhu XJ, Huang AL, Chen YZ, Wang XF (2015) Mesoporous carbon spheres: synthesis, surface modification and neutral red adsorption. Mater Lett 161:656–660
11. Liu YH, Yu QM, Liu X, Liu RJ (2019) Adsorption characteristics of methyl blue onto magnetic $Mn_{0.5}Co_{0.5}Fe_2O_4$ nanoparticles prepared via a rapid combustion process. Environ Prog Sustain 38: S277–S287
12. Bououdina M, Al-Najar B, Falamarzi L, Vijaya JJ, Shaikh MN, Bellucci S (2019) Effect of annealing on phase formation, microstructure and magnetic properties of $MgFe_2O_4$ nanoparticles for hyperthermia. Eur Phys J Plus. https://doi.org/10.1140/epjp/i2019-12485-5
13. Zhang Y, Zhou ZF, Wen FF, Tan J, Peng T, Lou BQ, Wang HG, Yin SX (2018) A flower-like MoS_2-decorated $MgFe_2O_4$ nanocomposite: mimicking peroxidase and colorimetric detection of H_2O_2 and glucose. Sens Actuat B-Chem 275:155–162
14. Ali NA, Yahya MS, Mustafa NS, Sazelee NA, Idris NH, Ismail M (2019) Modifying the hydrogen storage performances of $NaBH_4$ by catalyzing with $MgFe_2O_4$ synthesized via hydrothermal method. Int J Hydrog Energ 44:6720–6727
15. Wang SF, Li DM, Yang CQ, Sun GG, Zhang J, Xia YH, Xie CM, Yang GX, Zhou M, Liu W (2017) A novel method for the synthesize of nanostructured $MgFe_2O_4$ photocatalysts. J Sol-Gel Sci Techn 84(1):169–179
16. Ivanets A, Roshchina M, Srivastava V, Prozorovich V, Dontsova T, Nahirniak S, Pankov V, Hosseini-Bandegharaei A, Tran HN, Sillanpää M (2019) Effect of metal ions adsorption on the efficiency of methylene blue degradation onto $MgFe_2O_4$ as Fenton-like catalysts. Colloid Surf A 571:17–26
17. Yu QM, Wang Z, Zhang YW, Liu RJ (2019) Covalent immobilization and characterization of penicillin G acylase on amino and GO functionalized magnetic $Ni_{0.5}Zn_{0.5}Fe_2O_4@SiO_2$ nanocomposite prepared via a novel rapid-combustion process. Int J Biol Macromol 134:507–515
18. Liu X, Liu RJ, Pan S, Huang W, Fan MM, Li YJ (2019) A facile sol combustion and gel calcination process for the preparation of magnetic $MnFe_2O_4$ nanoparticles. J Nanosci Nanotechno 19:5790–5795
19. Yu QM, Pan S, Huang W, Liu RJ (2019) Effects of solution concentration on magnetic $NiFe_2O_4$ nanomaterials prepared via the rapid combustion process. J Nanosci Nanotechno 19:2449–2452
20. Liu RJ, Yu QM, Liu YH, Liu X, Wang FQ, Xu YN (2018) Optimization of citrate-gel preparation process for magnetic Ni-zn ferrite nanoparticles. J Nanosci Nanotechno 18:2838–2843
21. Doroftei C, Leontie L (2019) The influence of Sc^{3+} ions on the microstructure, electrical, and gas-sensing properties of Ni–Co–Sc ferrite. J Sol-Gel Sci Techn 91(3):654–663
22. Li SS, Liu QF, Lu RZ, Wu XY, Chen J(2018) Effect of solution concentration on magnetic $Ni_{0.5}Zn_{0.5}Fe_2O_4$ nanoparticles and their adsorption behavior of neutral red J Nanosci Nanotechnol 18:4798–4804
23. Khan MI, Akhtar S, Zafar S, Shaheen A, Khan MA, Luque R, Rehman AU (2015) Removal of Congo red from aqueous solution by anion exchange membrane (EBTAC): adsorption kinetics and themodynamics. Materials 8:4147–4161
24. Yang K, Sun Y (2007) Kinetics of adsorption on carbon from solutions. Biochem Eng J 37:298–310
25. Sayğılı GA (2015) Synthesis, characterization and adsorption properties of a novel biomagnetic composite for the removal of Congo red from aqueous medium. J Mol Liq 211:515–526
26. Ding Z, Wang W, Zhang YJ, Li F, Liu JP (2015) Synthesis, characterization and adsorption capability for Congo red of $CoFe_2O_4$ ferrite nanoparticles. J Alloy Compd 640:362–370
27. Jia ZG, Liu JH, Wang QZ, Li SB, Qi Q, Zhu RS (2015) Synthesis of 3D hierarchical porous iron oxides for adsorption of Congo red from dye wastewater. J Alloy Compd 622:587–595
28. Lafi R, Charradi K, Djebbi MA, Amara ABH, Hafiane A (2016) Adsorption study of Congo red dye from aqueous solution to Mg-Al-layered double hydroxide. Adv Powder Technol 27:232–237
29. Ji LF, Yu S, Zhou X, Bao YK, Yang FC, Kang WD, Zhang X (2019) Modification of electron structure on the semiconducting single-walled carbon nanotubes for effectively electrosensing guanine and adenine. Anal Chim Acta 1079:86–93
30. Jawad AH, Mubarak NSA, Abdulhameed AS (2019) Tunable Schiff's base-cross-linked chitosan composite for the removal of reactive red 120 dye: adsorption and mechanism study. Int J Biol Macromol. https://doi.org/10.1016/j.ijbiomac.2019.10.014
31. Pereira IC, Carvalho KQ, Passig FH, Ferreira RC, Rizzo-Domingues RCP, Hoppen MI, Perretto F (2018) Thermal and thermal-acid treated sewage sludge for the removal of dye reactive red 120: characteristics, kinetics, isotherms, thermodynamics and response surface methodology design. J Environ Chem Eng 6 (6):7233–7246
32. Prola LD, Acayanka E, Lima EC, Umpierres CS, Vaghetti JC, Santos WO, Djifon PT (2013) Comparison of Jatropha curcas shells in natural form and treated by non-thermal plasma as biosorbents for removal of reactive red 120 textile dye from aqueous solution. Ind Crop Prod 46:328–340
33. Jawad AH, Mamat NFH, Hameed BH, Ismaila K (2019) Biofilm of cross-linked chitosan-ethylene glycol diglycidyl ether for

removal of reactive red 120 and methyl orange: adsorption and mechanism studies. J Environ Chem Eng 7(2):102965
34. Tabak A, Baltas N, Afsin B, Emirik M, Caglar B, Erend E (2010) Adsorption of reactive red 120 from aqueous solutions by cetylpyridinium-bentonite. J Chem Technol Biot 85:1199–1207
35. Absalan G, Asadi M, Kamran S, Sheikhian L, Goltz DM (2011) Removal of reactive red-120 and 4-(2-pyridylazo) resorcinol from aqueous samples by Fe_3O_4 magnetic nanoparticles using ionic liquid as modifier. J Hazard Mater 192:476–484
36. Pérez-Calderón J, Santosa MV, Zaritzky N (2018) Reactive RED 195 dye removal using chitosan coacervated particles as bio-sorbent: analysis of kinetics, equilibrium and adsorption mechanisms. J Environ Chem Eng 6(5):6749–6760
37. Dehghani MH, Dehghan A, Najafpoor A (2017) Removing Reactive Red 120 and 196 using chitosan/zeolite composite from aqueous solutionS: kinetics, isotherms, and process optimization. J Ind Eng Chem 51(25):185–195